Atmos. Meas. Tech. Discuss., doi:10.5194/amt-2016-262, 2016
Manuscript under review for journal Atmos. Meas. Tech.
Published: 2 September 2016

Atmospheric Measurement Techniques Discussions

Monitoring Aerosol–Cloud Interactions at CESAR Observatory in the Netherlands

K. Sarna and H.W.J. Russchenberg

TU Delft Climate Institute, Faculty of Civil Engineering and Geotechnology, Delft University of Technology, Stevinweg 1, 2628 CN, Delft, The Netherlands

Correspondence to: Karolina Sarna (k.sarna@tudelft.nl)

Abstract. The representation of aerosol–cloud interactions (ACI) processes in the climate models, although long studied, still remains the source of high uncertainty. Very often there is a mismatch between the scale of observations used for ACI quantification and the ACI process itself. This can be changed by using the observations from ground-based remote sensing instruments. In this paper we presented a direct application of the Aerosol–Cloud Interactions monitoring technique (ACI monitoring). ACI monitoring is based on the standardized Cloudnet data stream, which provides measurements from ground-based remote sensing instruments working in synergy. For the dataset collected at the CESAR Observatory in the Netherlands we calculate ACI metrics. We use specifically attenuated backscatter coefficient (ATB) for the characterisation of the aerosol properties and cloud droplets effective radius (r_e) and number concentration (N_d) for the characterisation of the cloud properties. We calculate two metrics: $\mathrm{ACI_r} = \ln(r_\mathrm{e})/\ln(ATB)$ and $\mathrm{ACI_N} = \ln(N_\mathrm{d})/\ln(ATB)$. The calculated values of $\mathrm{ACI_r}$ were ranging from 0.016 to 0.17, which corresponds to the values reported in previous studies. We also evaluated impact of the updraft and liquid water path (LWP) on ACI metrics. The values of $\mathrm{ACI_r}$ were highest for the LWP between 50 and 100 $\mathrm{g/m^2}$. For the higher LWP other processes, such as collision and coalescence, seem to be dominant and obscure the ACI processes. We also saw that the values of $\mathrm{ACI_r}$ are higher when only data points located in the updraft area are considered. The method presented in this study enables monitoring aerosol–cloud interactions daily and further aggregating daily data into bigger datasets.

Atmos. Meas. Tech. Discuss., doi:10.5194/amt-2016-262, 2016
Manuscript under review for journal Atmos. Meas. Tech.
Published: 2 September 2016

Atmospheric Measurement Techniques Discussions

1 Introduction

Clouds are one of the most important systems of regulating Earth's radiation. Through changes in their macro- and microphysical properties clouds can significantly effect climate (Ramaswamy et al., 2001). Aerosol and their ability to act as cloud condensation nuclei can alter cloud microphysical properties. Twomey (1977) was the first one to postulate that the increasing pollution, later represented by aerosol concentration, will lead to an increasing cloud droplets concentration and a decreasing cloud droplets size. The effect of those microphysical changes is an increased albedo of clouds. Despite the good understanding of the physical principles of the aerosol–cloud interactions (ACI) processes, their representation in the climate models remains the source of the highest uncertainty (IPCC, 2014).

The conceptual process in which aerosol become activated into cloud droplets is well understood (Stephens, 1978; Lamb and Verlinde, 2011). Also, the influence of the aerosol concentration on the cloud microphysical properties, i.e. cloud droplets size and number concentration, has been studied extensively over the past decades (Feingold et al., 2003; Twohy et al., 2005; Kim et al., 2008; McComiskey et al., 2009) and its existence is not in question. The biggest uncertainty still lies with the scale of the process and it's importance over different locations and in different meteorological conditions. McComiskey and Feingold (2012) identified the mismatch in the scale of the ACI process and in the scale of the observations as one of the largest drivers of uncertainty in quantifying ACI. One possible way of overcoming this problem is by using the observations from ground-based remote sensing instruments. Ground-based remote sensing instruments are uniquely predisposed to provide high temporal resolution of measurements continuously. At the same time, they can examine the effect of aerosol concentration on cloud in a single air column and at the scale of the cloud droplets formation.

In the past years several studies used measurements from ground-based remote sensing instruments to quantify ACI (e.g., Feingold et al., 2003; Garrett et al., 2004; Pandithurai et al., 2009; Schmidt et al., 2015). The scope of instruments and measured parameters still differs among them. Further, a great majority of ACI studies is focused on the marine or coastal environment. Although harder to observe, ACI over continents is important to make a link between anthropogenic aerosol and the climate change through the ACI process.

A new approach to monitor ACI based on the standardize data format was proposed by Sarna and Russchenberg (2016). Their method (hereafter refereed to as ACI monitoring) is based on the Cloudnet data (Illingworth et al., 2007), a unified data format that is available across the Cloudnet network observatories. ACI monitoring also supplied an open-source software (Sarna, 2015) to process data from any Cloudnet station. In this paper we applied this method directly to the dataset from the CESAR (Cabauw Experimental Site for Atmospheric Research) Observatory.

The structure of this paper is as follows. First we present shortly the theoretical framework for calculations. Following by a description of the CESAR Observatory and the used dataset. Then we characterize ACI over CESAR Observatory and describe different drivers of the ACI process at this station. We finish with a summary and conclusions.

Atmos. Meas. Tech. Discuss., doi:10.5194/amt-2016-262, 2016
Manuscript under review for journal Atmos. Meas. Tech.
Published: 2 September 2016

Atmospheric Measurement Techniques Discussions

2 Theoretical basis of aerosol–cloud interactions

The relation between aerosol concentrations and the cloud droplets size was first postulated by Twomey (1974). Using airborne measurements he showed that an increasing pollution, and hence an increasing concentration of CCN, will result in clouds with a higher optical thickness. That is measureable only if all other parameters, mainly the amount of available water represented by the liquid water path (*LWP*), are kept the same. Cloud optical thickness can be related to both the cloud albedo and cloud microphysical properties. Cloud optical thickness (τ_d) is proportional both to the cloud droplets number concentration (N_d):

$$\tau_d \propto N_d^{1/3} \tag{1}$$

(Twomey, 1974), and to the cloud droplets effective radius (r_e):

$$\tau_d \propto \frac{LWP}{r_e} \tag{2}$$

(Stephens, 1978).

The increasing pollution that Twomey (1974) referred to is now represented by aerosol background. Proxies used to define the aerosol background vary between studies and include parameters such as: aerosol number concentration (N_a), aerosol optical thickness (τ_a), or aerosol index.

The relation between N_d and N_a was postulated first based on the experimental studies by Twomey and Warner (1967) as

$$N_d \propto N_a^{\gamma}, \tag{3}$$

where γ is the proportionality factor. The theoretical values of γ vary between 1 and 0. To account for γ, Feingold et al. (2003) introduced the indirect effect index, which hereafter will be refereed to as ACI metric. It was defined as a relative change in the cloud properties due to changes in the aerosol properties. In the form that directly relates to Eq.3 we can say that

$$ACI_N = \frac{d\ln N_d}{d\ln \alpha} \quad 0 < ACI_N < 1, \tag{4}$$

where α is any of the above mentioned proxies of the aerosol properties. The value of ACI_N can be related to the value of γ. To relate aerosol properties to cloud droplets size Feingold et al. (2003) used

$$ACI_r = -\left.\frac{d\ln r_e}{d\ln \alpha}\right|_{\mathrm{LWP}} \quad 0 < ACI_r < 0.33, \tag{5}$$

where r_e is the cloud droplets effective radius. The bounds of ACI_r between 0 and 0.33 stem from the assumption of a constant *LWP* when using r_e. ACI_N is traditionally not bound by the values of *LWP* as it's associated with the activation process which has no direct microphysical relation to *LWP* (McComiskey et al., 2009). The relation between ACI_r and ACI_N is described as:

$$ACI_r = \frac{1}{3} ACI_N. \tag{6}$$

Mathematically, both ACI_r and ACI_N are defined as a slope of the regression line between the logarithm of the aerosol property and the logarithm of the cloud property. We can define a linear regression between aerosol and cloud property as:

$$ln(cloud) = a + m ln(aerosol) \tag{7}$$

Atmos. Meas. Tech. Discuss., doi:10.5194/amt-2016-262, 2016
Manuscript under review for journal Atmos. Meas. Tech.
Published: 2 September 2016

Atmospheric Measurement Techniques Discussions

where m is the slope defined as:

$$m = r_{aerosol,cloud}\frac{s_{cloud}}{s_{aerosol}}, \tag{8}$$

where $r_{aerosol,cloud}$ is the Pearson product-moment correlation coefficient between *ln(aerosol)* and *ln(cloud)*, s_{cloud} is the standard deviation of *ln(cloud)* and $s_{aerosol}$ is the standard deviation of *ln(aerosol)*. The correlations coefficient $r_{aerosol,cloud}$ is defined as:

$$r_{aerosol,cloud} = \frac{cov(aerosol, cloud)}{s_{aerosol}s_{cloud}}. \tag{9}$$

cov(aerosol,cloud) is the covariance between *ln(aerosol)* and *ln(cloud)*. In this study we use ACI monitoring scheme which relies both on the calculation of the correlation coefficient and ACI metrics (ACI_N and ACI_r).

3 Methodology of ACI monitoring scheme

As we mentioned in previous sections, in this paper we use the Aerosol–Cloud Interaction (ACI) monitoring scheme as described in Sarna and Russchenberg (2016). The core of this method is the Cloudnet dataset. It provides a standardized data stream from ground-based remote sensing instruments working in synergy. In specific, it includes measurements from cloud radar, lidar and microwave radiometer. Although this is a set of instruments present at all observatories within the Cloudnet network, their specification may vary from station to station.

Cloudnet dataset was designed to facilitate retrieval of microphysical cloud properties. Therefore, a retrieved values of cloud droplets effective radius (r_e) and cloud droplets number concentration (N_d) are available from the dataset. The microphysical retrieval method used in the Cloudnet dataset is based on the method designed by Frisch et al. (2002). In this paper we use the Frisch et al. (2002) retrieval with the assumptions of homogeneous mixing as described in Knist (2014). The aerosol background is represented in the ACI monitoring scheme by an integrated value of the attenuated backscatter coefficient (*ATB*). The value is integrated from the height of a complete overlap (Kovalev, 2015), which is 120 m in the setup of this study, to 300 m below the cloud base.

3.1 Data selection criteria

Due to the use of cloud microphysical properties the ACI monitoring scheme is applicable only in specific conditions. In particular, only low-level liquid water clouds in well-mixed conditions can be considered. The cloud base should be located below 2000 m above ground level (AGL), a limit used for the classification of low-level clouds. Due to the integrations of *ATB* only clouds with cloud base located above 500 m AGL are considered. This is because the complete overlap is at 120 m and data is only considered up to 300 m below the cloud. *ATB* should be integrated through at least 2 range gates of the used lidar, which for most Cloudnet observatories are 40 m wide. Other criteria include presence of precipitation or drizzle. The Cloudnet dataset contains target classification where liquid cloud droplets are categorized specifically (Hogan and O'Connor, 2004). ACI monitoring scheme selects only data points where liquid cloud droplets and aerosol are identified. All other data

Atmos. Meas. Tech. Discuss., doi:10.5194/amt-2016-262, 2016
Manuscript under review for journal Atmos. Meas. Tech.
Published: 2 September 2016

points are disregarded.

For the dataset used in this study we aggregated daily data into one dataset. The data aggregation is only possible if data was collected in similar meteorological conditions. We define the meteorological conditions on the basis of temperature and pressure. We considered conditions to be similar if the relative standard deviation (rsd) of the measurements is less than 0.1. The relative standard deviation is defined as a ratio of the standard deviation of the dataset to the mean of the dataset. Additional meteorological parameter that we use is the specific humidity. However, the changes in the specific humidity can be larger than those in temperature or pressure. A parameter which controls the constant conditions of the available water is the liquid water path (*LWP*). All selected data points are divided into bins of *LWP*, where each bin is 10 $\mathrm{g/m^2}$ wide. It should be noted that meteorological conditions available in the Cloudnet dataset come from the KNMI (Koninklijk Nederlands Meteorologisch Instituut) regional atmospheric climate model RACMO (Van Meijgaard et al., 2008) and not from the observations.

4 Observations from CESAR Observatory

The CESAR (Cabauw Experimental Site for Atmospheric Research) Observatory is located in the Netherlands (51.971° N, 4.927° E) in an area located 0.7 m below the mean sea level. The site is equipped with a large set of instruments providing constant measurements to study atmospheric processes. The dataset used in this study was collected in October - November 2014 during the ACCEPT (Analysis of the Composition of mixed-phase Clouds with Extended Polarization Techniques) campaign. Although ACCEPT campaign was focused on mixed-phase clouds, multiple measurements of low-level liquid water clouds were also collected. During the six weeks period of the campaign seven days were represented by a persisting layer of Stratocumulus clouds. Due to the requirements of the ACI monitoring scheme, after applying data selection criteria (see Section 3.1) only four days of data were processed. The total amount of measurements profiles used in this study is 1664. We used one additional requirement to choose them: we only processed profiles where the Stratocumulus layer was persisting for at least 30 minutes. This meant that we only chose data were at least 60 profiles of 30 sec integrated measurements were consecutive. We chose to add this selection criteria to eliminate from the aggregated dataset days were only a couple of profiles responding to all selection criteria were available.

4.1 Instrumentation

One of the main objectives of the ACI monitoring scheme was to develop a method that can be easily applied at various observatories. To achieve that it was necessary to base this method on a widely spread set of instruments. Those instruments include cloud radar, lidar and microwave radiometer. In this study we used specifically data from: (1) a Ka-band 35.5 GHz Cloud radar MIRA, (2) a CHM15X ceilometer operating at 1064 nm and (3) HATPRO (Humidity and Temperature Profiler) microwave radiometer (MWR) operating at 14 frequencies - 7 frequencies between 22 and 31 GHz (K-band) and 7 frequencies between 51 and 58 GHz (V-Band). Data from cloud radar MIRA and HATPRO MWR is used for the retrieval of cloud microphysical properties, specifically cloud droplets effective radius r_e and cloud droplets number concentration N_d. Both microphysical parameters are retrieved in accordance with Knist (2014). Data is re-sampled to an uniform time-height resolution. Time res-

Atmos. Meas. Tech. Discuss., doi:10.5194/amt-2016-262, 2016
Manuscript under review for journal Atmos. Meas. Tech.
Published: 2 September 2016

olution is 30 seconds and height resolution (range gate) is 31.2 meters. Moreover, cloud radar MIRA measures the Doppler velocity, which is used to measure updraft within the cloud. Data from HATPRO MWR is also used to measure liquid water path (*LWP*), which is used to divide data into bins. This division is made in order to consider data in conditions approaching constant amount of water available. In principle the size of *LWP* bins should be as small as possible. In order to have a representable data sample we make each bin 10 $\mathrm{g/m^2}$ wide. Finally, data from CHM15X ceilometer is used to measure the aerosol concentration. We use the integrated value of the attenuated backscatter coefficient (*ATB*) as a proxy of the aerosol concentration. Table 1 summarises all used parameters and the instruments that were used to measure and/or retrieve them.

4.2 Aerosol background at CESAR

A limited amount of studies of ACI processes was focused until now on the continental low-level liquid water clouds (e.g., Feingold et al., 2003; Ahmad et al., 2013). Most studies were focused on marine or coastal liquid water clouds (e.g., McComiskey et al., 2009; Pandithurai et al., 2009; Twohy et al., 2005). The CESAR Observatory is located in the western part of the Netherlands. The liquid water clouds observed over CESAR have characteristics of continental clouds. Further, the aerosol background is typically continental. Aerosol over CESAR are mainly represented by an organic aerosol as well as high concentration of ammonium nitrate (Mensah et al., 2012). This type of aerosol background is important to study as it can be directly related to the anthropogenic emissions (Putaud et al., 2004).

4.3 Selected dataset

As we mentioned in the previous sections, due to the microphysical scale of the ACI processes data need to be aggregated only in similar meteorological conditions (as defined in Section 3.1). This is to make sure that ACI processes is not obscured by other meteorological processes. Figure 1 presents histograms of the meteorological conditions of the aggregated dataset. The values of pressure and temperature show small variation, represented by a small value of the relative standard deviation (rsd), 0.03 for pressure and 0.01 for temperature. The variation of specific humidity is larger, with rsd of 0.22. However, to secure that the amount of available water is constant, we divide data into bins of *LWP*. It is important to note that for the Cloudnet dataset meteorological conditions are provided by the KNMI Regional Atmospheric Climate Model (RACMO) (Van Meijgaard et al., 2008).

The histograms of all measured and retrieved parameters used in this study, as summarised in Table 1, for the selected dataset are presented on Figure 2. It is important to note that for the calculation of ACI metric (as defined in Eq. 5 and Eq. 4) r_e, N_d and *ATB* are logarithmically transformed. By calculating the logarithmic slope we are accounting for the relative response of r_e and N_d to changes in aerosol (*ATB*).

We use an additional measurement from cloud radar, the Doppler velocity, to measure updraft and downdraft. The ACI metrics are expected to be stronger in the updraft areas as that's where aerosol is activated into cloud droplets. Figure 3 presents the histogram of Doppler velocity in the aggregated dataset. Note that we use the average measure of the updraft from the cloud base to two gate ranges within the cloud.

Atmos. Meas. Tech. Discuss., doi:10.5194/amt-2016-262, 2016
Manuscript under review for journal Atmos. Meas. Tech.
Published: 2 September 2016

Atmospheric Measurement Techniques Discussions

5 Results and discussion

5.1 ACI metrics

ACI metrics are calculated for the aggregated dataset from CESAR Observatory. We check the response of cloud microphysical properties (r_e and N_d) to aerosol properties (aerosol concentration is represented by *ATB*). To accurately quantify ACI the amount of available water should be kept constant. To meet this requirement we divide data into bins of *LWP*. Each *LWP* bin is 10 gm^{-2} wide. Calculations are made for the bins between 30 and 150 gm^{-2}. The lower limit of the *LWP* analysis range was chosen as twice the error of the HATPRO MWR measurements (15 gm^{-2}). The upper limit is the precipitation threshold. For every *LWP* bin we also calculate the Pearson product-moment correlation coefficient, r (Eq. 9).

5.1.1 $\mathrm{ACI_r}$

To calculate $\mathrm{ACI_r}$ we used Eq. 5. Figure 4 presents scatter plots of r_e and *ATB*. Each panel corresponds to a *LWP* bin and presents the corresponding value of $\mathrm{ACI_r}$ and correlation coefficient, r. The range of values within the physical limits (between 0 and 0.33, see Section 2) is from 0.016 to 0.171. This values are in agreement with other studies concerned with quantifying $\mathrm{ACI_r}$ in continental clouds. Kim et al. (2008) reported values of $\mathrm{ACI_r}$ between 0.04 and 0.17 in a study over the ground-based remote sensing site at the Southern Plains in Oklahoma, USA. For the same site, Feingold et al. (2003) reported values of $\mathrm{ACI_r}$ between 0.02 and 0.16.

In the dataset from CESAR Observatory we can see that values of $\mathrm{ACI_r}$ are generally within the physical limits for the *LWP* values from 30 to 110 gm^{-2}. This may indicate that $\mathrm{ACI_r}$ is only a significant process in certain *LWP*s and for the higher values other processes within the cloud, such as collision and coalescence for example, are dominant and obscure the ACI process. To further investigate the impact of *LWP* on $\mathrm{ACI_r}$ we selected only the profiles which were corresponding to the updraft area. This was done based on the Doppler velocity. Figure 5 presents scatter plots of r_e and *ATB* for every bin in the updraft area. Firstly, it's important to note that the dataset is significantly limited when considering only the updraft area. However, we observe a considerable increase in the value of both $\mathrm{ACI_r}$ and the correlation coefficient, r. Table 2 compares the calculated values of $\mathrm{ACI_r}$ and the correlation coefficient, r, for the whole dataset and for the updraft area only. Again, we can see that the values of $\mathrm{ACI_r}$ are higher for the smaller values of *LWP*. $\mathrm{ACI_r}$ seems to be most significant for the values of *LWP* between 50 and 100 gm^{-2}. Note that for *LWP* above 100 gm^{-2} values of $\mathrm{ACI_r}$ are also high in the updraft area, however the sample size is too small for those bins to draw any relevant conclusions.

5.1.2 $\mathrm{ACI_N}$

The response of the cloud droplets concentration to the aerosol background is an approximation of the activation process. $\mathrm{ACI_N}$ can be directly linked to Eq. 3. We calculate the relative change of N_d with the change of *ATB* from Eq. 4. For the aggregated dataset from CESAR Observatory the value of $\mathrm{ACI_N}$ is 0.19. Figure 6 presents the scatter plot of N_d and *ATB*. The value of 0.19 is very small, often values reported in the literature vary between 0.48 and 0.99 (McComiskey et al., 2009, and

Atmos. Meas. Tech. Discuss., doi:10.5194/amt-2016-262, 2016
Manuscript under review for journal Atmos. Meas. Tech.
Published: 2 September 2016

Atmospheric Measurement Techniques Discussions

references within). However, it has been noted before that the size of aerosol may influence the value of ACI_N. Smaller aerosol size tends to yield smaller ACI_N (McComiskey et al., 2009). Based on the aerosol background at the CESAR Observatory (see Section 4.2) we expect a smaller size of the aerosol particles. It is also important to note that the retrieval of N_d has very high estimated uncertainties, ranging between 40 and 60% (Knist, 2014). Those uncertainties are mainly due to the instruments and algorithms errors. By comparison, the uncertainty of the r_e ranges between 10 and 15%. We suspect that this high uncertainty is responsible for the low value of ACI_N calculated for the whole dataset.

As we mentioned above, based on the theoretical relationships between aerosol and cloud droplets ACI_N is not dependent on the *LWP*. However, in this study we decided to test if there is a dependence of ACI_N on the *LWP* by dividing data into the same bins of *LWP* as with the calculation of ACI_r. Figure 7 presents the scatter plots of N_d and *ATB* divided into bins of *LWP*. What is striking, is that same as in the case of ACI_r the highest values of ACI_N are present in the range between 50 and 110 gm^{-2}. We further selected only the points within the updraft areas. Table 3 presents the comparison of the ACI_N calculated for each *LWP* bin for the whole dataset and only for the updraft areas. Again, consistently with ACI_r, the highest values of ACI_N are noted for the *LWP* between 60 and 80 gm^{-2}.

ACI_N and ACI_r are theoretically related as in Eq. 6. In the dataset analysed in this study this relation is not always present. We expect that the main reason for that is the high uncertainty of the N_d retrieval. Also, ACI_N is harder to measure Based on this study, we can say that ACI_r seems to give more realistic results as they are broadly in agreement with the previous studies (see Section 5.1.1).

5.2 Impact of the updraft

Activation of the aerosol particles into cloud droplets is invigorated in the updraft zones (Altaratz et al., 2014). In this study we identified updraft areas with the use of the Doppler velocity (w). Tables 2 and 3 compare the results of ACI_r and ACI_N calculated for all *LWP* bins. Both parameters seem to indicate stronger relation between cloud properties (r_e and N_d) and aerosol properties (*ATB*) in the updraft areas. This is implicated by the increase of both the ACI metrics as well as the correlation coefficients. It is important to note that the amount of available profiles is greatly diminished by the selection of updraft areas only. In the aggregated dataset from the CESAR Observatory roughly one-fourth of the profiles is located in the updraft areas. The number of samples in *LWP* bins over 100 gm^{-2} is too small to make significant conclusions. However, we can clearly observe that both ACI_r and ACI_N have the highest values in the *LWP* bins between 60 and 80 gm^{-2}.

5.3 Relation with *LWP*

One of the conditions for observing changes in microphysical properties of clouds due to an increasing pollution (later represented by aerosol) initially postulated by Twomey (1977) was the constant amount of water available. Over the past decades different studies used that conditions with liberty. In the satellite remote-sensing quantification of ACI the constraint of *LWP* is often omitted (e.g., Kaufman et al., 2005). In the ground-based remote sensing methods the *LWP* constraint is kept, but the size of *LWP* bins varies greatly. The division into *LWP* bins is important as it is still not clear if ACI is a significant process in different *LWP* regimes.

Atmos. Meas. Tech. Discuss., doi:10.5194/amt-2016-262, 2016
Manuscript under review for journal Atmos. Meas. Tech.
Published: 2 September 2016

Atmospheric Measurement Techniques Discussions

In this study we decided to divide data into *LWP* bins 10 gm^{-2} wide. The values of *LWP* we consider are between 30 and 150 gm^{-2}. Values of $\mathrm{ACI_r}$ are plotted against *LWP* on Figure 8. We observe an increase of $\mathrm{ACI_r}$ with *LWP* in the range between 30 and 100 gm^{-2}. If we makes same comparison for the updraft areas only (Figure 9) we get similar results, with an exception of *LWP* between 30 and 50 gm^{-2}, where $\mathrm{ACI_r}$ reaches values out of bounds. Further, the updraft only dataset suggests that $\mathrm{ACI_r}$ is strongest for *LWP* between 60 and 80 gm^{-2}. For the higher values of *LWP* the ACI processes are most probably obscured by collision and coalescence.

5.4 Relation between correlation coefficient (*r*) and $\mathrm{ACI_r}$

Most of the studies concerned with aerosol–cloud interactions calculate either $\mathrm{ACI_r}$ (Eq. 5), $\mathrm{ACI_N}$ (Eq. 4) or both to quantify the relationship between aerosol and cloud properties. As we explained before, in mathematical terms $\mathrm{ACI_r}$ and $\mathrm{ACI_N}$ are a slope of the regression line calculated between natural logarithm of the aerosol properties and a natural logarithm of the cloud properties. The aerosol property is treated as the independent variable and the cloud property is the dependent variable. As we explained in Section 2, correlation coefficient and slope of the regression line are related as in Eq. 8.

For the dataset from the CESAR Observatory we compared the values of $\mathrm{ACI_r}$ with the values of the correlation coefficient. We did this comparison for every *LWP* bin for the whole dataset and then separately only for the profiles corresponding to the updraft area and to the downdraft area. Figure 10 presents the scatter plot between $\mathrm{ACI_r}$ and the correlation coefficient. We observe higher values of both $\mathrm{ACI_r}$ and the correlation coefficient in the updraft areas. We also observe that most of the values of $\mathrm{ACI_r}$ outside of the physical bounds are observed for the downdraft areas of the whole dataset. This further underlines the impact of the updraft on the aerosol–cloud interactions. Moreover, most of the values outside of the physical bounds of $\mathrm{ACI_r}$, regardless of the updraft or downdraft zone, are observed for either high or very low values of LWP (above 110 and lower than 50 $\mathrm{g/m^2}$). This again indicates importance of the value of LWP for the evaluation of the aerosol–cloud interactions processes. The relation between the correlation coefficient and $\mathrm{ACI_r}$ is mathematically sound, however, not often presented in the literature. This relation between the two parameters is only significant when data is sampled at a high temporal and spatial resolution and divided into bins of *LWP*. In case of no constraint on *LWP* or data with a low spatial resolution (i.e. satellite remote sensing aggregated datasets) the calculation of the correlation coefficient will become irrelevant, as the variance of the dataset will be minimized by the aggregation (McComiskey and Feingold, 2012). In case of the ACI monitoring scheme calculating both $\mathrm{ACI_r}$ and the correlation coefficient is relevant, as data is collected with a temporal and spatial resolution that corresponds to the scale of the aerosol–cloud interactions processes.

6 Summary and conclusions

In this paper we presented a direct application of the Aerosol–Cloud Interactions monitoring scheme as presented in (Sarna and Russchenberg, 2016). We used Cloudnet dataset from the CESAR Observatory in the Netherlands. Data were collected during the ACCEPT measuring campaign in October - November 2014. We aggregated daily measurements into one dataset

Atmos. Meas. Tech. Discuss., doi:10.5194/amt-2016-262, 2016
Manuscript under review for journal Atmos. Meas. Tech.
Published: 2 September 2016

Atmospheric Measurement Techniques Discussions

based on the similar meteorological conditions. We only considered non-precipitating low-level liquid water clouds. All forms of precipitation where disregarded based on the Cloudnet target categorisation. Investigated clouds had the cloud base located between 500 and 2000 m above ground level. Lastly, we only used periods when conditions corresponding to the above mentioned criteria were persisting for at least 30 minutes.

For the aggregated dataset we calculated ACI metrics using cloud droplets effective radius (r_e) following Eq. 5 and cloud droplets number concentration (N_d) following Eq. 4. The aerosol properties where represented by the integrated attenuated backscatter coefficient (*ATB*). For both ACI metrics we also calculate Pearson's moment correlation coefficient, r. For all the above mentioned calculations data were divided into bins of liquid water path (*LWP*), where every bin was 10 $\mathrm{g/m^2}$ wide. The calculated values of $\mathrm{ACI_r}$ were ranging from 0.016 to 0.17, which widely corresponds to the values reported in previous studies. The values of $\mathrm{ACI_N}$ where significantly lower than those reported in the literature. We attribute that to two reasons. Firstly, the retrieval of N_d is susceptible to high error, varying between 40 and 60% due to instrument errors and retrieval assumptions. Secondly, the aerosol background over the CESAR Observatory is characteristic of the continental aerosol background whereas most studies calculating $\mathrm{ACI_N}$ are located in the marine or coastal areas. The size of continental aerosol is significantly smaller which can lead to smaller values of $\mathrm{ACI_N}$. Considering high uncertainty of N_d retrieval, we recommend the calculation of $\mathrm{ACI_r}$ for accounting the impact of aerosol on the cloud microphysics.

We also evaluated impact of the updraft and LWP on ACI metrics. In the analyzed dataset both of those parameters showed clear impact on the values of $\mathrm{ACI_r}$. The values of $\mathrm{ACI_r}$ were highest for the LWP between 50 and 100 $\mathrm{g/m^2}$. For the higher values of LWP other processes, such as collision and coalescence, seem to be dominant and obscure the ACI processes. We also saw that the values of $\mathrm{ACI_r}$ are higher when only data points located in the updraft area are considered. As indicated in previous studies, the updraft is an important factor in invigorating aerosol–cloud interactions. The values of $\mathrm{ACI_r}$ in the downdraft area were often outside of the physical bounds. It is desirable to only consider data points located in the updraft. However, it should be noted that selection of updraft areas only significantly decreases the data sample.

The ACI metrics is used to account for the proportionality factor between aerosol number concentration and cloud droplet number concentration (Eq. 3). In this study we explained that the correlation coefficient and ACI metrics can be related for the high-resolution dataset, as ACI metric is the slope of the regression line between cloud and aerosol properties. We observed a decrease of the correlation coefficient with the increase of the $\mathrm{ACI_r}$. We observed an inverse relation between aerosol and cloud properties therefore lower value of correlation coefficient indicates higher dependency of the parameters.

The method presented in this study enables monitoring aerosol–cloud interactions daily and further aggregating daily data into bigger datasets. We showed that it can be easily implemented at any observatory using Cloudnet data format. A wide-spread network of aerosol–cloud interactions monitoring could lead to estimating more accurately the drivers of this process in various conditions. This methodology can be integrated into the Cloudnet network products. Further, as the methodology presented here is based on the remote-sensing instruments only, it could be adapted to the satellite remote sensing. Such an adaptation would have to be done with care and account for all the requirements of the data selection necessary for this method.

Atmos. Meas. Tech. Discuss., doi:10.5194/amt-2016-262, 2016
Manuscript under review for journal Atmos. Meas. Tech.
Published: 2 September 2016

Atmospheric Measurement Techniques Discussions

Acknowledgements. The research leading to these results has received funding from the European Union Seventh Framework Programme (FP7/2007-2013) under grant agreement 262254.

The authors would like to acknowledge and thank dr. Patric Seifert from Leibniz-Institut für Troposphärenforschung (TROPOS) and Lukas Pfitzenmaier from Delft University of Technology for providing the dataset from the ACCEPT campaign used in this study.

Atmos. Meas. Tech. Discuss., doi:10.5194/amt-2016-262, 2016
Manuscript under review for journal Atmos. Meas. Tech.
Published: 2 September 2016

Atmospheric Measurement Techniques Discussions

References

Ahmad, I., Mielonen, T., Grosvenor, D. P., Portin, H. J., Arola, A., Mikkonen, S., Kühn, T., Leskinen, A., Joutsensaari, J., Komppula, M., Lehtinen, K. E. J., Laaksonen, A., and Romakkaniemi, S.: Long-term measurements of cloud droplet concentrations and aerosol–cloud interactions in continental boundary layer clouds, Tellus B, 65, doi:10.3402/tellusb.v65i0.20138, http://www.tellusb.net/index.php/tellusb/article/view/20138/30541, 2013.

Altaratz, O., Koren, I., Remer, L., and Hirsch, E.: Review: Cloud invigoration by aerosols—Coupling between microphysics and dynamics, Atmospheric Research, 140-141, 38–60, doi:10.1016/j.atmosres.2014.01.009, http://linkinghub.elsevier.com/retrieve/pii/S0169809514000106, 2014.

Feingold, G., Eberhard, W. L., Veron, D. E., and Previdi, M.: First measurements of the Twomey indirect effect using ground-based remote sensors, Geophys. Res. Lett., 30, 1287, doi:10.1029/2002GL016633, 2003.

Frisch, S., Shupe, M., Djalalova, I., Feingold, G., and Poellot, M.: The Retrieval of Stratus Cloud Droplet Effective Radius with Cloud Radars, J. Atmos. Oceanic Technol., 19, 835–842, doi:10.1175/1520-0426(2002)019<0835:TROSCD>2.0.CO;2, 2002.

Garrett, T. J., Zhao, C., Dong, X., Mace, G. G., and Hobbs, P. V.: Effects of varying aerosol regimes on low-level Arctic stratus, Geophys. Res. Lett., 31, L17 105, doi:10.1029/2004GL019928, 2004.

Hogan, R. J. and O'Connor, E. J.: Facilitating cloud radar and lidar algorithms: the Cloudnet Instrument Synergy/Target Categorization product, 2004.

Illingworth, A. J., Hogan, R. J., O'Connor, E. J., Bouniol, D., Delanoë, J., Pelon, J., Protat, A., Brooks, M. E., Gaussiat, N., Wilson, D. R., Donovan, D. P., Baltink, H. K., van Zadelhoff, G.-J., Eastment, J. D., Goddard, J. W. F., Wrench, C. L., Haeffelin, M., Krasnov, O. A., Russchenberg, H. W. J., Piriou, J.-M., Vinit, F., Seifert, A., Tompkins, A. M., and Willén, U.: Cloudnet, Bull. Amer. Meteor. Soc., 88, 883–898, doi:10.1175/BAMS-88-6-883, 2007.

IPCC, ed.: Climate Change 2013 - The Physical Science Basis: Working Group I Contribution to the Fifth Assessment Report of the Intergovernmental Panel on Climate Change, Cambridge University Press, Cambridge, 2014.

Kaufman, Y. J., Koren, I., Remer, L. A., Rosenfeld, D., and Rudich, Y.: The effect of smoke, dust, and pollution aerosol on shallow cloud development over the Atlantic Ocean, PNAS, 102, 11 207–11 212, doi:10.1073/pnas.0505191102, 2005.

Kim, B.-G., Miller, M. A., Schwartz, S. E., Liu, Y., and Min, Q.: The role of adiabaticity in the aerosol first indirect effect, J. Geophys. Res., 113, D05 210, doi:10.1029/2007JD008961, 2008.

Knist, C. L.: Retrieval of liquid water cloud properties from ground-based remote sensing observations, Ph.D. thesis, TU Delft: Civil Engineering and Geosciences: Geoscience and Remote Sensing, 2014.

Kovalev, V. A.: Solutions in LIDAR Profiling of the Atmosphere, John Wiley & Sons, 2015.

Lamb, D. and Verlinde, J.: Physics and Chemistry of Clouds, Cambridge University Press, 2011.

McComiskey, A. and Feingold, G.: The scale problem in quantifying aerosol indirect effects, Atmos. Chem. Phys., 12, 1031–1049, doi:10.5194/acp-12-1031-2012, 2012.

McComiskey, A., Feingold, G., Frisch, A. S., Turner, D. D., Miller, M. A., Chiu, J. C., Min, Q., and Ogren, J. A.: An assessment of aerosol-cloud interactions in marine stratus clouds based on surface remote sensing, J. Geophys. Res., 114, D09 203, doi:10.1029/2008JD011006, 2009.

Mensah, A. A., Holzinger, R., Otjes, R., Trimborn, A., Mentel, T. F., ten Brink, H., Henzing, B., and Kiendler-Scharr, A.: Aerosol chemical composition at Cabauw, The Netherlands as observed in two intensive periods in May 2008 and March 2009, Atmospheric Chemistry and Physics, 12, 4723–4742, doi:10.5194/acp-12-4723-2012, http://www.atmos-chem-phys.net/12/4723/2012/, 2012.

Pandithurai, G., Takamura, T., Yamaguchi, J., Miyagi, K., Takano, T., Ishizaka, Y., Dipu, S., and Shimizu, A.: Aerosol effect on cloud droplet size as monitored from surface-based remote sensing over East China Sea region, Geophysical Research Letters, 36, L13 805, doi:10.1029/2009GL038451, http://doi.wiley.com/10.1029/2009GL038451, 2009.

Putaud, J.-P., Raes, F., Van Dingenen, R., Brüggemann, E., Facchini, M.-C., Decesari, S., Fuzzi, S., Gehrig, R., Hüglin, C., Laj, P., Lorbeer, G., Maenhaut, W., Mihalopoulos, N., Müller, K., Querol, X., Rodriguez, S., Schneider, J., Spindler, G., ten Brink, H., Tørseth, K., and Wiedensohler, A.: A European aerosol phenomenology—2: chemical characteristics of particulate matter at kerbside, urban, rural and background sites in Europe, Atmospheric Environment, 38, 2579–2595, doi:10.1016/j.atmosenv.2004.01.041, http://www.sciencedirect.com/science/article/pii/S1352231004000949, 2004.

Ramaswamy, V., Chanin, M.-L., Angell, J., Barnett, J., Gaffen, D., Gelman, M., Keckhut, P., Koshelkov, Y., Labitzke, K., Lin, J.-J. R., O'Neill, A., Nash, J., Randel, W., Rood, R., Shine, K., Shiotani, M., and Swinbank, R.: Stratospheric temperature trends: Observations and model simulations, Reviews of Geophysics, 39, 71–122, doi:10.1029/1999RG000065, http://doi.wiley.com/10.1029/1999RG000065, 2001.

Sarna, K.: ACI monitoring: First release, doi:10.5281/zenodo.32033, 2015.

Sarna, K. and Russchenberg, H. W. J.: Ground-based remote sensing scheme for monitoring aerosol–cloud interactions, Atmospheric Measurement Techniques, 9, 1039–1050, doi:doi:10.5194/amt-9-1039-2016, http://www.atmos-meas-tech.net/9/1039/2016/, 2016.

Schmidt, J., Ansmann, A., Bühl, J., and Wandinger, U.: Strong aerosol–cloud interaction in altocumulus during updraft periods: lidar observations over central Europe, Atmospheric Chemistry and Physics, 15, 10 687–10 700, doi:10.5194/acp-15-10687-2015, http://www.atmos-chem-phys.net/15/10687/2015/acp-15-10687-2015.html, 2015.

Stephens, G. L.: Radiation Profiles in Extended Water Clouds. II: Parameterization Schemes, J. Atmos. Sci., 35, 2123–2132, doi:10.1175/1520-0469(1978)035<2123:RPIEWC>2.0.CO;2, 1978.

Twohy, C. H., Petters, M. D., Snider, J. R., Stevens, B., Tahnk, W., Wetzel, M., Russell, L., and Burnet, F.: Evaluation of the aerosol indirect effect in marine stratocumulus clouds: Droplet number, size, liquid water path, and radiative impact, J. Geophys. Res., 110, D08 203, doi:10.1029/2004JD005116, 2005.

Twomey, S.: Pollution and the planetary albedo, Atmos. Environ., 8, 1251–1256, doi:10.1016/0004-6981(74)90004-3, 1974.

Twomey, S.: The Influence of Pollution on the Shortwave Albedo of Clouds, J. Atmos. Sci., 34, 1149–1152, doi:10.1175/1520-0469(1977)034<1149:TIOPOT>2.0.CO;2, 1977.

Twomey, S. and Warner, J.: Comparison of Measurements of Cloud Droplets and Cloud Nuclei, J. Atmos. Sci., 24, 702–703, doi:10.1175/1520-0469(1967)024<0702:COMOCD>2.0.CO;2, 1967.

Van Meijgaard, E., Van Ulft, L., Van de Berg, W., Bosveld, F., Van den Hurk, B., Lenderink, G., and Siebesma, A.: The KNMI regional atmospheric climate model RACMO version 2.1, Koninklijk Nederlands Meteorologisch Instituut, 2008.

Atmos. Meas. Tech. Discuss., doi:10.5194/amt-2016-262, 2016
Manuscript under review for journal Atmos. Meas. Tech.
Published: 2 September 2016

Atmospheric Measurement Techniques Discussions

Table 1. Cloud and Aerosol Properties Measured or Derived From the Observations at the CESAR Observatory in the Netherlands.

Measured Quantity	Definition	Instrument(s)
Cloud Liquid Water Path	LWP ($\mathrm{gm^{-2}}$)	HATPRO MWR
Radar Reflectivity Factor	Z (dBZ or $\mathrm{m^6m^{-3}}$)	MIRA
Doppler Velocity	w ($\mathrm{ms^{-1}}$)	MIRA
Cloud Droplet Effective Radius	r_e (μm) (Knist, 2014)	MIRA/HATPRO MWR
Cloud Droplet Number Concentration	N_d ($\mathrm{cm^{-3}}$) (Knist, 2014)	MIRA/HATPRO MWR
Attenuated Backscatter Coefficient	ATB [$\mathrm{m^{-1}sr^{-1}}$]	CHM15X ceilometer

Table 2. ACI_r (Eq. 5) together with Pearson product-moment correlation coefficient, r, calculated between ln(r_e) and ln(ATB) calculated for the aggregated dataset. Data is divided in to bins of LWP. ACI_r is calculated for the whole dataset and only for the updraft areas. The number of measurements in each bin (n) is also presented.

	Whole dataset			Only updraft		
LWP bin	ACI_r	r	n	ACI_r	r	n
$30 < LWP < 40$	0.02	-0.04	342	-0.09	0.24	125
$40 < LWP < 50$	-0.03	0.07	291	-0.05	0.12	86
$50 < LWP < 60$	0.04	-0.08	256	0.03	-0.06	83
$60 < LWP < 70$	0.06	-0.12	175	0.26	-0.45	46
$70 < LWP < 80$	0.07	-0.16	175	0.22	-0.33	47
$80 < LWP < 90$	-0.04	0.08	102	0.14	-0.36	24
$90 < LWP < 100$	0.09	-0.20	89	0.16	-0.45	29
$100 < LWP < 110$	0.17	-0.30	84	0.17	-0.48	12
$110 < LWP < 120$	-0.08	0.14	45	0.25	-0.82	11
$120 < LWP < 130$	-0.01	0.02	40	-0.03	0.06	12
$130 < LWP < 140$	-0.04	0.06	38	0.06	-0.12	13
$140 < LWP < 150$	-0.06	0.16	27	-0.29	0.74	4

Atmos. Meas. Tech. Discuss., doi:10.5194/amt-2016-262, 2016
Manuscript under review for journal Atmos. Meas. Tech.
Published: 2 September 2016

Atmospheric Measurement Techniques Discussions

Table 3. ACI_N (Eq. 4) together with Pearson product-moment correlation coefficient, r, calculated between $\ln(N_d)$ and $\ln(ATB)$ calculated for the aggregated dataset. Data is divided in to bins of *LWP*. ACI_N is calculated for the whole dataset and only for the updraft areas. The number of measurements in each bin (n) is also presented.

	Whole dataset			Only updraft		
LWP bin	ACI_N	r	n	ACI_N	r	n
30 < *LWP* < 40	0.05	-0.04	342	-0.10	-0.08	125
40 < *LWP* < 50	-0.01	0.07	291	-0.04	-0.04	86
50 < *LWP* < 60	0.37	-0.08	256	0.05	0.04	83
60 < *LWP* < 70	0.48	-0.12	175	0.52	0.27	46
70 < *LWP* < 80	0.39	-0.16	175	0.80	0.44	47
80 < *LWP* < 90	0.26	0.08	102	0.00	0.00	24
90 < *LWP* < 100	0.29	-0.20	89	0.33	0.26	29
100 < *LWP* <110	0.16	-0.30	84	0.39	0.22	12
110 < *LWP* <120	-0.11	0.14	45	-0.12	-0.15	11
120 < *LWP* <130	-0.23	0.02	40	-0.17	-0.14	12
130 < *LWP* <140	0.19	0.06	38	-0.10	-0.11	13
140 < *LWP* <150	0.08	0.16	27	0.75	0.52	4

Atmos. Meas. Tech. Discuss., doi:10.5194/amt-2016-262, 2016
Manuscript under review for journal Atmos. Meas. Tech.
Published: 2 September 2016

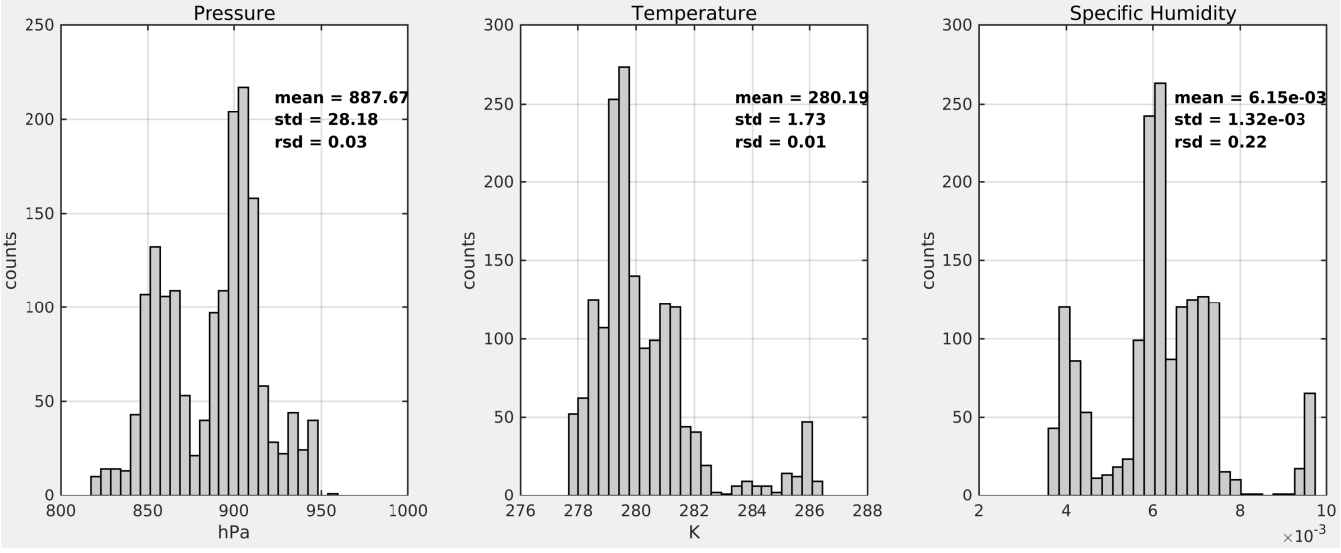

Figure 1. Histograms of the meteorological data for the aggregated dataset.

Atmos. Meas. Tech. Discuss., doi:10.5194/amt-2016-262, 2016
Manuscript under review for journal Atmos. Meas. Tech.
Published: 2 September 2016

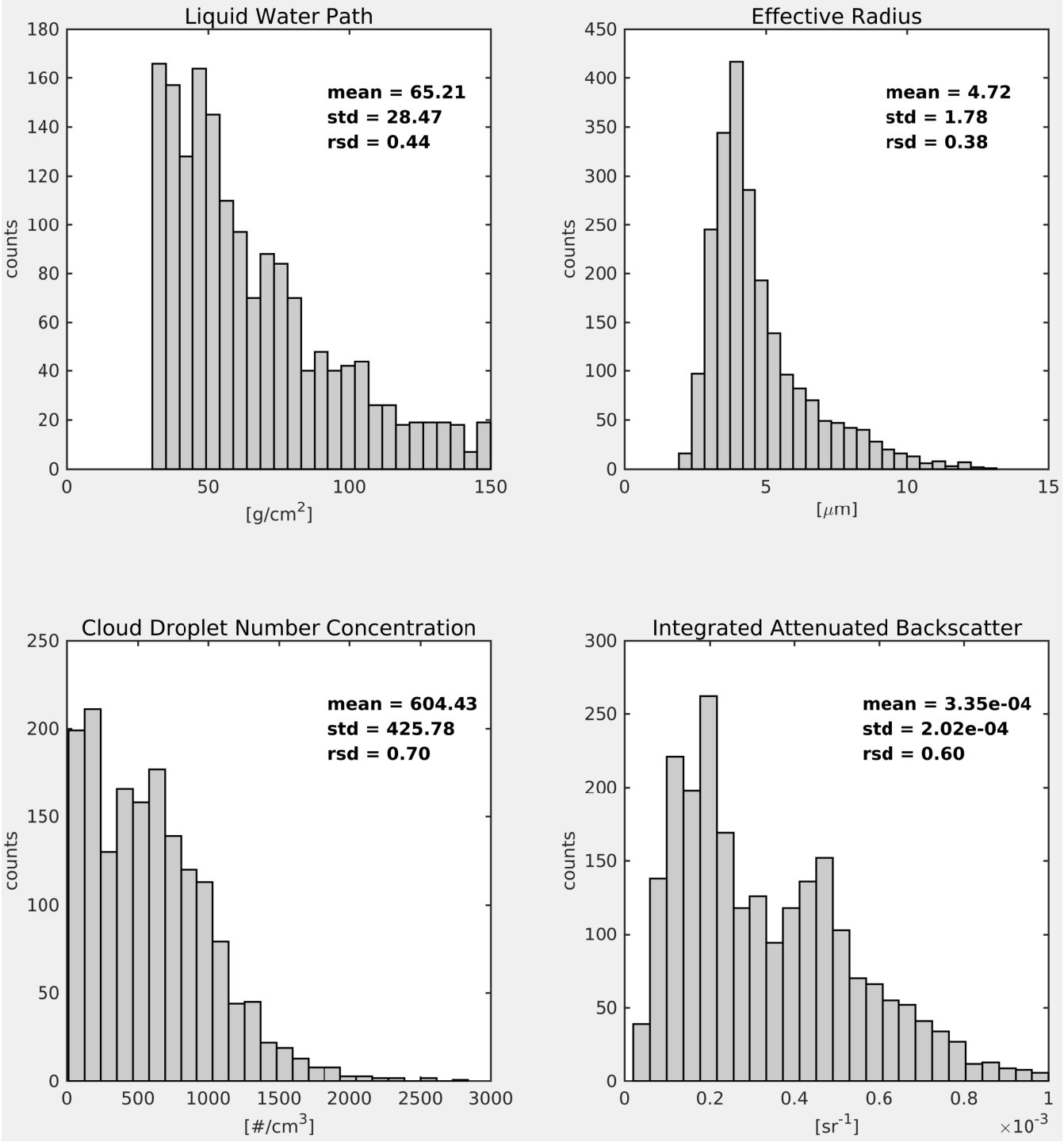

Figure 2. Histograms of the measurements and retrievals for the aggregated dataset.

Atmos. Meas. Tech. Discuss., doi:10.5194/amt-2016-262, 2016
Manuscript under review for journal Atmos. Meas. Tech.
Published: 2 September 2016

Atmospheric Measurement Techniques Discussions

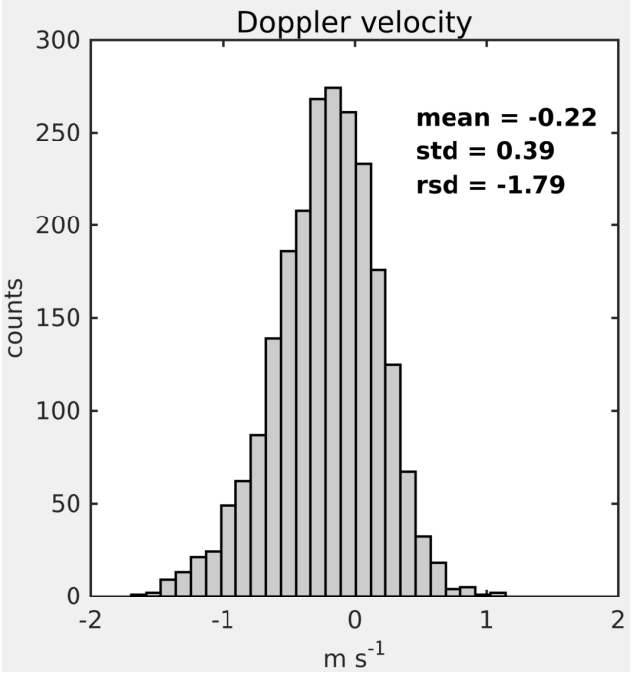

Figure 3. Histograms of the Doppler velocity for the aggregated dataset.

Atmos. Meas. Tech. Discuss., doi:10.5194/amt-2016-262, 2016
Manuscript under review for journal Atmos. Meas. Tech.
Published: 2 September 2016

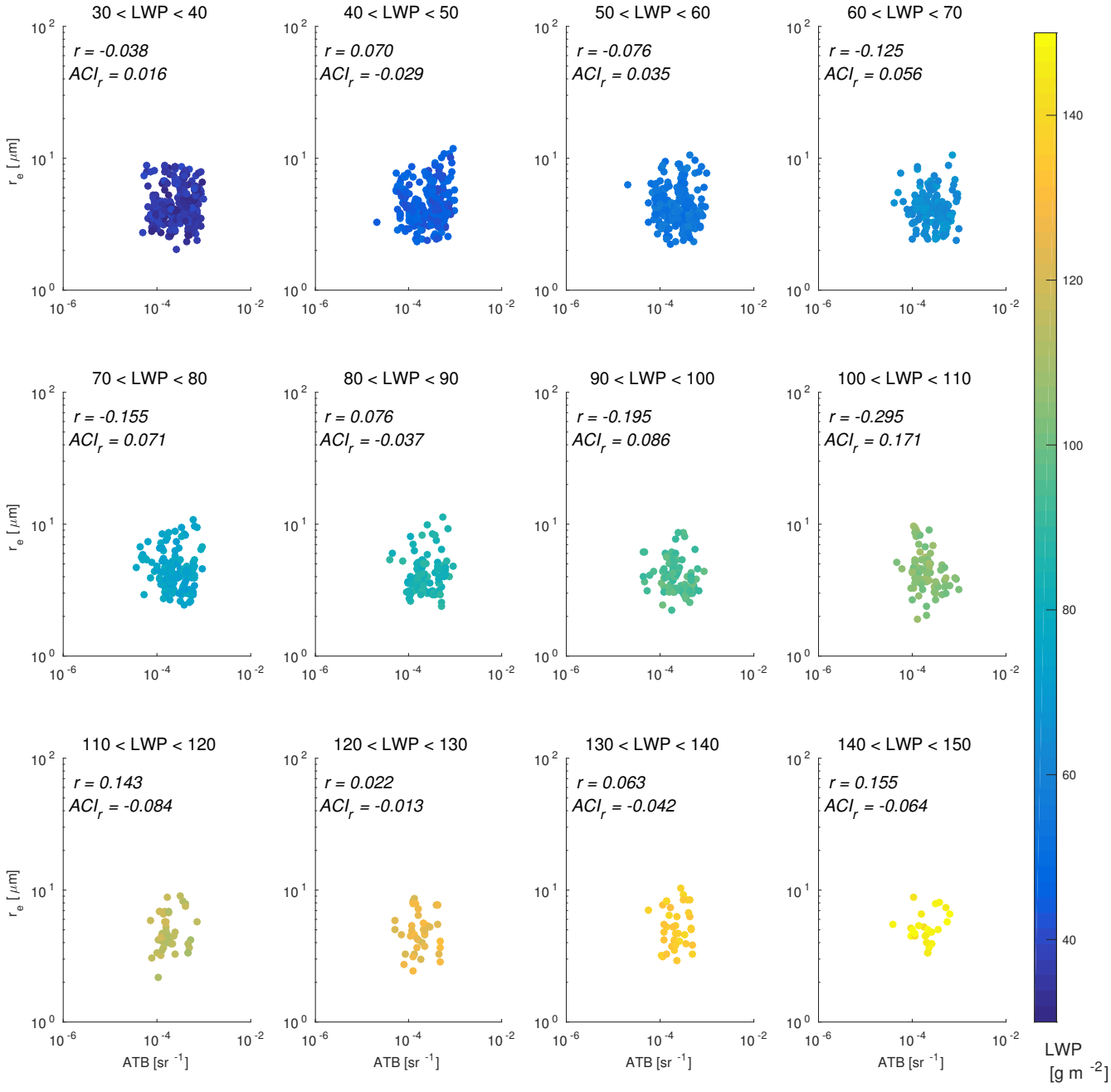

Figure 4. Scatter plots of the integrated attenuated backscatter coefficient and cloud droplets effective radius. This plots represent all data points from the aggregated dataset divided by the value of the liquid water path.

Atmos. Meas. Tech. Discuss., doi:10.5194/amt-2016-262, 2016
Manuscript under review for journal Atmos. Meas. Tech.
Published: 2 September 2016

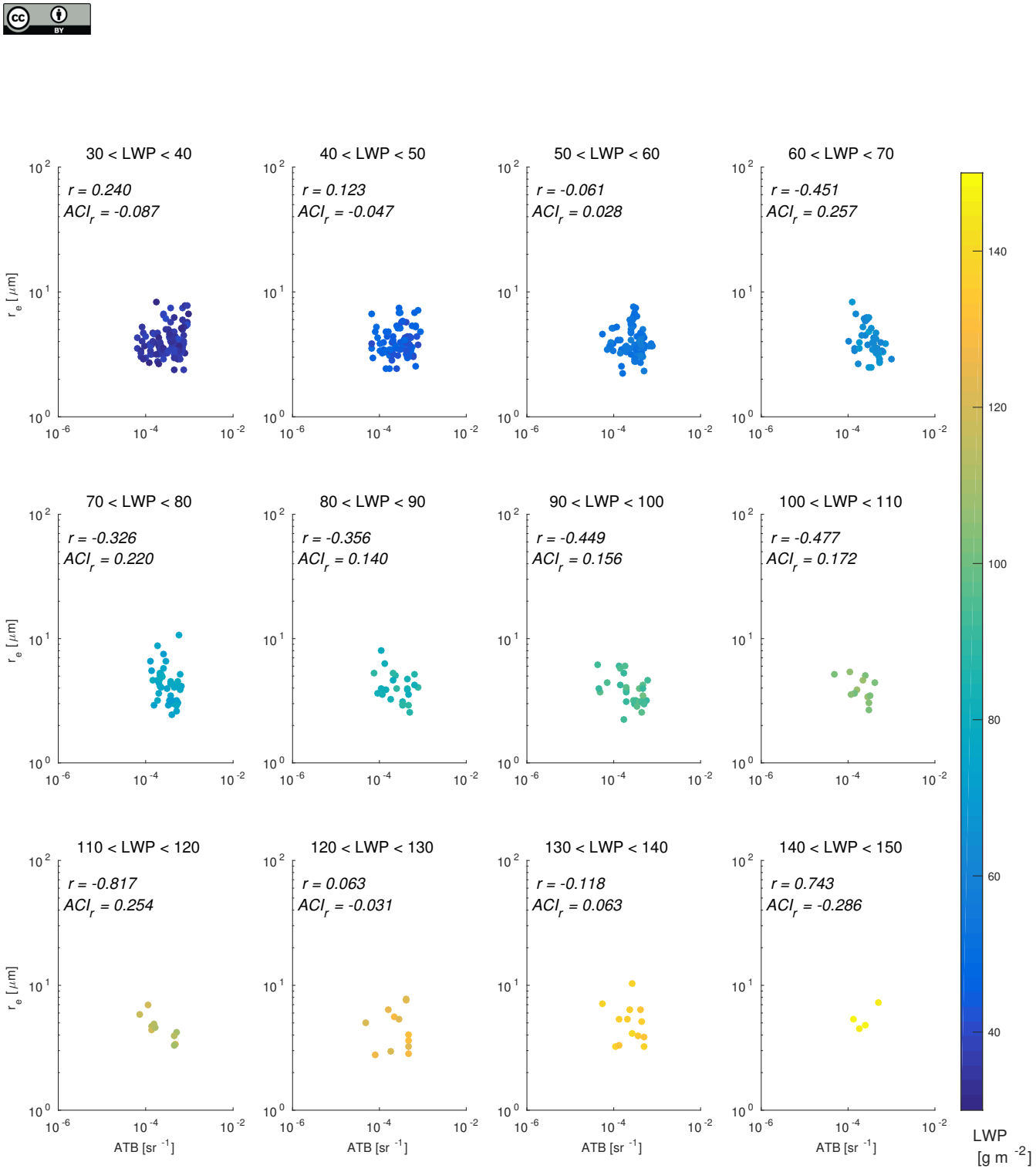

Figure 5. Scatter plots of the integrated attenuated backscatter coefficient and cloud droplets effective radius. This plots represent only data points from the updraft areas in the aggregated dataset divided by the value of the liquid water path. .

Atmos. Meas. Tech. Discuss., doi:10.5194/amt-2016-262, 2016
Manuscript under review for journal Atmos. Meas. Tech.
Published: 2 September 2016

Atmospheric Measurement Techniques Discussions

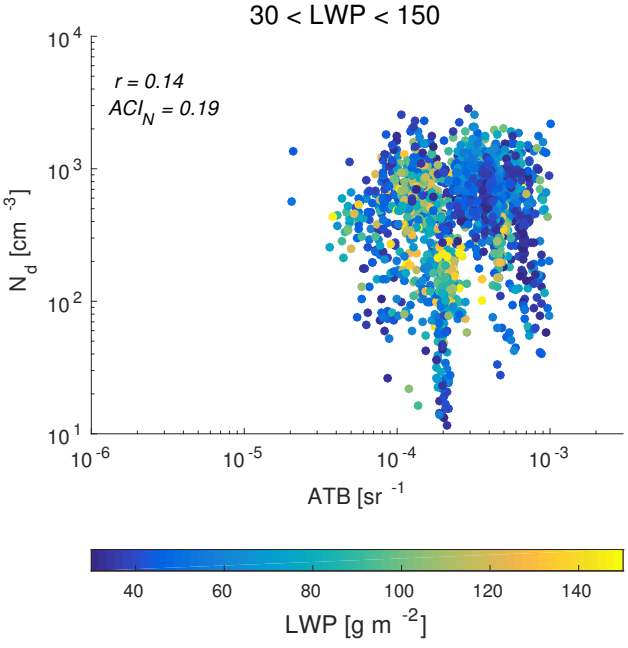

Figure 6. Scatter plot of integrated attenuated backscatter coefficient and the cloud droplets number concentrations. This plots represents all data points from the aggregated dataset.

Atmos. Meas. Tech. Discuss., doi:10.5194/amt-2016-262, 2016
Manuscript under review for journal Atmos. Meas. Tech.
Published: 2 September 2016

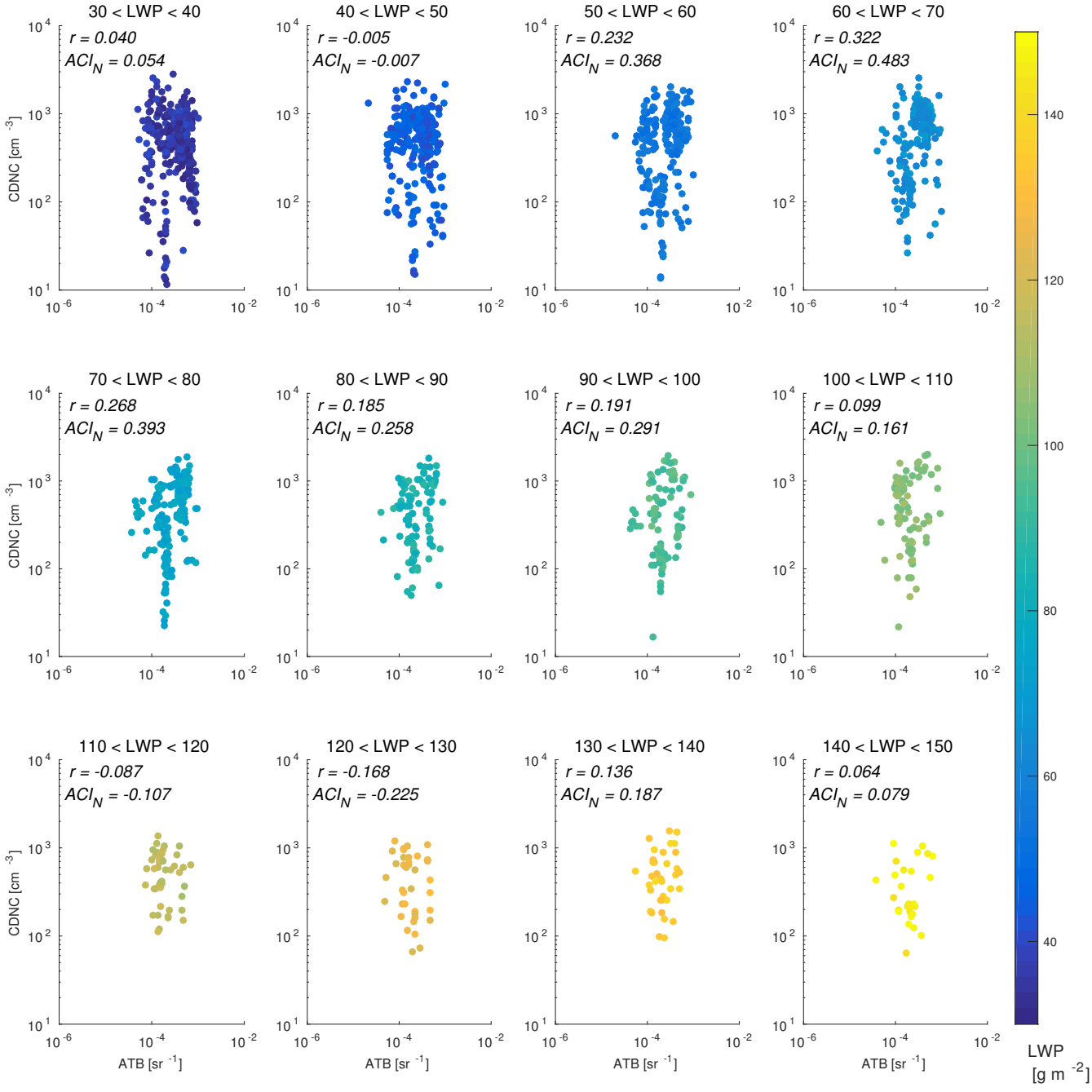

Figure 7. Scatter plots of integrated attenuated backscatter coefficient and the cloud droplets number concentrations divided by the value of the liquid water path. This plots represents all data points from the aggregated dataset.

Atmos. Meas. Tech. Discuss., doi:10.5194/amt-2016-262, 2016
Manuscript under review for journal Atmos. Meas. Tech.
Published: 2 September 2016

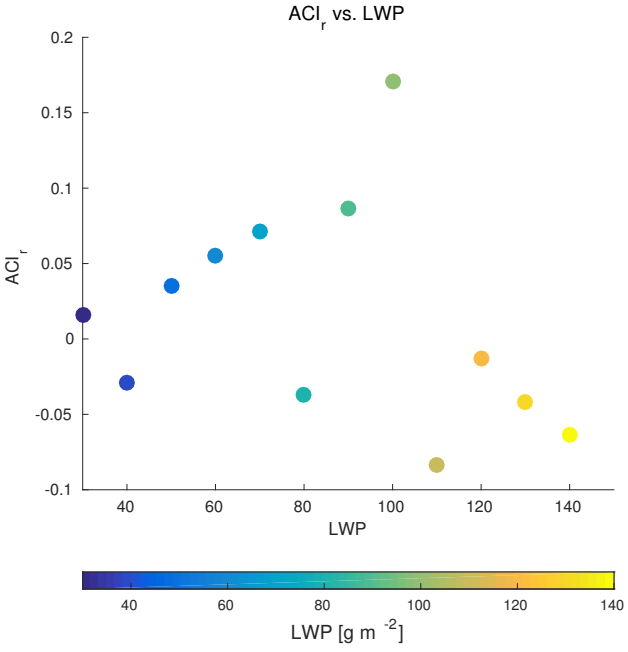

Figure 8. Scatter plot between ACI_r and *LWP*for all data points in the aggregated dataset.

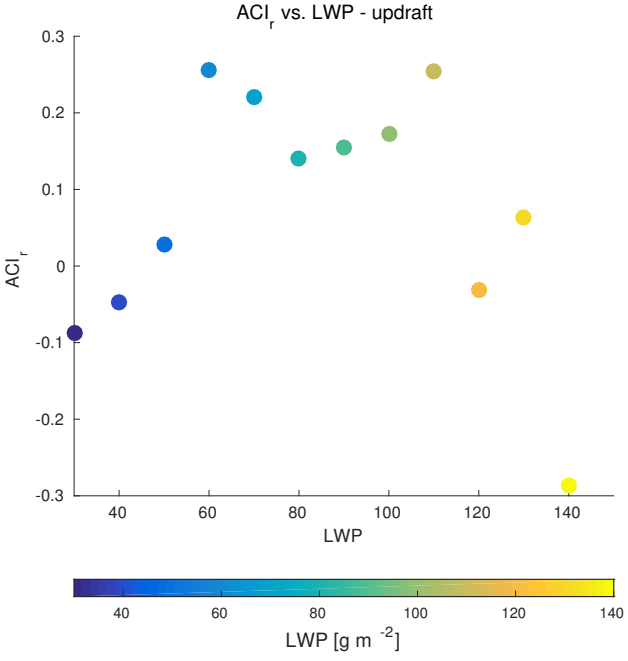

Figure 9. Scatter plot between ACI_r and *LWP* for the data points located in the updraft areas of the aggregated dataset.

Atmos. Meas. Tech. Discuss., doi:10.5194/amt-2016-262, 2016
Manuscript under review for journal Atmos. Meas. Tech.
Published: 2 September 2016

Atmospheric Measurement Techniques Discussions

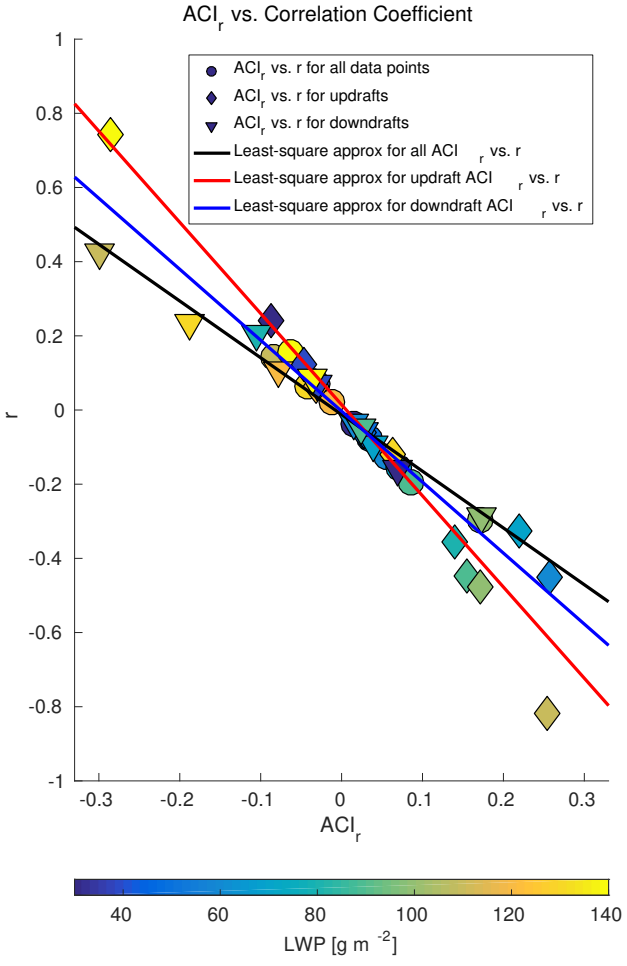

Figure 10. Scatter plot between ACI_r and the Pearson product-moment correlation coefficient, r.